Sorption, anomalous water transport and dynamic porosity in cement paste: a spatially localised ^{1}H NMR relaxation study and a proposed mechanism

Peter J. McDonald*, Ors Istok, Magdalena Janota, Agata M. Gajewicz-Jaromin, David A. Faux

Department of Physics, University of Surrey, Guildford, Surrey, GU2 7XH, UK

Abstract

The link between anomalous water sorption and dynamic porosity in cement pastes is explored using spatially resolved GARField ^{1}H nuclear magnetic resonance (NMR) relaxation analysis. A model is developed in which the effective capillary diffusion coefficient is dependent on the instantaneous pore size distribution. This and earlier data show changes in pore size distribution resultant from changes in saturation that do not occur instantaneously with changes in degree of saturation. Therefore, it is assumed that the pore size distribution is always relaxing exponentially towards a (saturation dependent) equilibrium. It follows that the diffusivity is sample history (*i.e.* time) dependent as well as saturation dependent. This is sufficient to explain anomalies in rapid capillary water sorption. The same concepts are applied to slow drying. In this case, porosity changes occur on a timescale much shorter than drying so the system is always in dynamic equilibrium and anomalies are therefore not seen.

*p.mcdonald@surrey.ac.uk

Keywords: water sorption, diffusion, cement paste, anomalous transport, NMR

1. Introduction

It is long known and well recognised that water transport in cement based materials is anomalous [1][2][3][4]. By this it is generally meant that water uptake or drying does not advance linearly with the square root of time, $t^{1/2}$, when otherwise expected. For instance, mass uptake of water from one end of a dry porous sample and the associated advance of the wetting front before that front reaches the opposite end of the sample normally proceeds as $t^{1/2}$. Equally, in the stages of drying experiments where the rate limiting step is transport of water to the drying surface rather than surface evaporation and while the opposite end of the sample remains saturated, mass loss proceeds as $t^{1/2}$. This $t^{1/2}$ behaviour is expected irrespective of whether the underlying transport mechanism is understood to be capillary action or diffusive: both can be formulated in a mathematical model in which the liquid flux is proportional to the local gradient of water saturation [5]. The constant of proportionality is a transport coefficient commonly known as the "diffusivity" with some adjective that indicates the mechanism. For capillary action, the transport coefficient is the capillary (hydraulic) diffusivity. It has units of [length]^2.[distance]$^{-1}$ and varies as the square of the sorptivity [5]. The $t^{1/2}$ behaviour is also expected whether or not the transport coefficient is a constant or a function of saturation so that a saturation-dependent diffusivity is not an indicator of anomalous transport. Further, anomalous transport is distinct from sorption hysteresis which is another characteristic of water in

cement. Moreover, the first sorption cycle of cementitious materials is generally found to be different to all subsequent sorption cycles [6] meaning that there is not only hysteresis but also first cycle irreversibility. While all three are distinct phenomena, it is increasingly probable that the three, anomalous transport, sorption hysteresis and first sorption cycle irreversibility, are linked at some low level of microstructural understanding.

There have been numerous possible explanations of anomalous transport in cement. Most trivial is delayed hydration. The idea here is that in an under-hydrated material, sorbed water causes further hydration, a densification of hydrates and a refinement of the porosity leading to a lower transport coefficient. This has long been known and was visualised using magnetic resonance imaging (MRI) over 20 years ago [7]. However, the fact that anomalous transport is seen in very well hydrated materials suggests that this is not a general explanation. Another possible interpretation is precipitation of calcium hydroxide leading to pore blocking. A liquid wetting front advancing into a sample carries with it ions. As the front advances, so it slows. There comes a point where the mass uptake of liquid equals the mass lost by evaporation at the wetting front and so the front stops. The ions precipitate at the liquid / vapour interface and lead to growth of solids that block the pathway. Evidence for this is seen in magnetic resonance imaging experiments on larger samples of mortar [8]. Following wetting and the observation of a stopped front, the sample is dried then re-wet from the other end. The new wetting front cannot progress beyond the blockage and so stops where the first did, while travelling in the opposite direction.

A large volume of data can be fit on the basis of two $t^{1/2}$ processes:

an initial fast one followed by a slower one. The crossover between different rates of ingress is generally found to be on the timescale of 6 to 24 hr. [9]. Micro-cracking offers an explanation consistent with this observation [4]. Shrinkage of a drying sample leads to the creation of micro-cracks. In subsequent sorption the cracks rapidly fill according to a fast $t^{1/2}$ process. Water then invades the surrounding matrix from the crack reservoirs according to a second, slower, $t^{1/2}$ process.

This leads to the explanations that variously invoke swelling. The basic concept for sorption is that water rapidly ingresses a micropore network due to normal capillary action. With time, the water migrates ("diffuses") from this network of pores into the surrounding smaller pores of the hydrate gel that swells. Like micro-cracking, swelling also introduces the idea of two $t^{1/2}$ processes: the faster one associated with the initial uptake and the slower one with the subsequent swelling by the water of the surrounding gel. The latter process is associated with macroscopic physical swelling suggesting that the volume of water that can be adsorbed increases. A variant of the idea was qualitatively set out by Saeidpour and Wadso [3]. It has been developed mathematically by Alderete and co-workers [10, 11]. Given that the model identifies that the initial sorption proceeds as $t^{1/2}$ and that the swelling also proceeds as $t^{1/2}$, it follows that that overall sorption proceeds as $t^{1/4}$. The model is able to describe a range of capillary sorption data.

We cannot discount the swelling model. However, from our perspective, there are fundamental objections that need to be answered before it can be widely accepted. First, the model presupposes that the initial sorption is into a network of "large" pores. Necessarily this must be a connected net-

work. Micrographs of pastes published by numerous authors in numerous studies do not suggest that capillary pores on the scale of microns or above are connected. The next pore size distribution downward are pores within the hydrate gel that are on the scale of 5 - 20 nm. We suggest that these pores are too connected to the smaller inter-layer porosity of the gel to allow the large separation of timescales required to see ingress that is not $t^{1/2}$. Our own work has previously suggested that the time required for exchange of water between inter-layer spaces and gel pores is measured in milli-seconds rather than in hours [12, 13], albeit in young pastes. Second, the model does not accommodate dynamic porosity. It is increasingly clear from NMR data, [14][15], and length-change isotherm data, [16], that the pore size distribution evolves in cements *subsequent* to changes in water saturation with at least one, two, and possibly three time constants measured on the scale of hours (pore collapse) to months (creep). So, while a significant amount of experimental data evidencing anomalous diffusion can be well fit on the basis of rapid initial uptake as $t^{1/2}$ with a large transport coefficient that transitions to a slower uptake with smaller transport coefficient again with a $t^{1/2}$ dependence, it is not self evident that this translates to a $t^{1/4}$ explanation notwithstanding that such data might be reasonably fit to a $t^{1/4}$ dependence especially if the possibility of small systematic offsets in time origin or early-onset end-effects are admitted.

Most recently, Hall, [17], has proposed an explanation based on a time dependent permeability, that, through the relationship between sorption coefficient and transport coefficient leads to a time dependent transport coefficient. Actually, this is not the first suggestion of this kind. Lockington and

Parlange made a similar suggestion many years earlier [18]. The key difference is that Lockington and Parlange have the transport coefficient varying with absolute time (*i.e.* from the start of sorption) whereas Hall has the time origin defined locally at the moment of arrival of the wetting front. The latter model avoids many of the philosophical / conceptual issues of the former that have been clearly laid out in [17]. Hall's ideas are much closer to the premise of this work. Hall supposes that in uptake experiments the time dependency arises from a refinement of the porosity that slows ingress. The solution of Hall's equations leads to a macro behaviour very similar to that suggested here. However, while Hall's model can be used for, for example, an empirical fit to mass uptake data, it does not include an underlying parametrisation of the time dependence that can be tested against experiment at a lower level.

This paper develops the idea of dynamic porosity as a mechanism of anomalous transport. It presents a mix of spatially-localised, time-resolved and filled porosity-distribution-resolved ^{1}H nuclear magnetic resonance (NMR) experimental data and numerical simulation in support of the idea. A new model is advanced. The model assumes that the transport coefficient at any one time and position is a function of the instantaneous local pore size distribution. It further recognises that there is a (measurable) multi-modal pore size distribution of constant total porosity that slowly, but continuously, relaxes towards an equilibrium dependent of the instantaneous water saturation [14]. Hence the transport coefficient is a function of concentration *and* time. The time dependency leads to the transport anomaly.

The experimental data differs from most cement transport data previously reported. Most commonly, gravimetric or similar data is available. If

spatially resolved data is recorded, then it is normally presented in the form of profiles or images: saturation as a function of position recored at a specific time. In this work, data are presented in the form of water saturation (by pore size) at a given location within the sample as a function of time which is the opposite way around. For normal diffusion, the two styles can be shown to be mathematically equivalent through the Boltzmann transformation and the variable, $\eta = x/2t^{1/2}$ [19]. For our purposes, the alternate format allows us to achieve much greater spatial resolution and retain high quality pore size discrimination with good time resolution also. The only work of which we are aware that acquires comparable ^{1}H NMR relaxation data in a similar manner is by Van Landeghem *et. al* [20] looking at cement paste using so-called stray field ^{1}H NMR imaging and an NMR-MOUSE and also by Schulte-Hothausen *et. al* [21] looking at mortar using an NMR-MOUSE. Both record local changing filled porosity distributions during wetting or drying. Schulte-Hothausen *et. al* qualitatively interpret the observations in terms of local hydrate swelling but without a link to transport.

The paper is laid out as follows. Section 2 presents the new theory; section 3 presents the experimental and modelling details; section 4 presents the experimental results and analysis. The paper ends with a wider discussion and conclusion.

2. Theory

The dominant mechanism of liquid water uptake into cement is capillary sorption. Water is drawn into the matrix by a contact line force at the liquid / air interface at the sorption front. However, ahead of the front and within

partially filled pores behind the front, vapour diffusion is also important. One might also reasonably argue that liquid diffusion within the nano-porous gel, especially within the sub nanometre inter-layer spaces of the gel hydrates that link between gel pores, is also a valid possible mechanism. Notwithstanding this apparent complexity, a basic transport equation is written as

$$J = -D\frac{\partial s}{\partial x} \tag{1}$$

leading to

$$\frac{\partial s}{\partial t} = \frac{\partial}{\partial x}\left(D\frac{\partial s}{\partial x}\right) \tag{2}$$

where x and t are position and time variables respectively; s is the water saturation; and D is the transport coefficient that may be a function of s. In the absence of gravity or other similar force acting, for a semi-infinite system either drying or wetting from one end, these equations lead to $t^{1/2}$ behaviour measured either gravimetrically or by distance of travel of the liquid water-air interface.

When a system comprises a composite of two or more materials, then an effective transport coefficient, D_{eff}, may be defined for transport over length scales large to the scale of the composite heterogeneity. When the fluid passes serially from one material to the next then the effective coefficient is given by

$$\frac{1}{D_{\text{eff}}} = \sum \frac{\phi_{\text{i}}}{D_{\text{i}}} \tag{3}$$

where D_{i} is the coefficient and ϕ_{i} the volume fraction of the i^{th} material component. We observe that cement porosity has a multi-modal pore size distribution. Let us consider that the dominant material through which water moves is the gel and that there are three critical pore sizes: smaller

than about 1 nm (hydrate inter-layer spaces); about 3-5 nm (gel pores) and larger than 5 nm (inter-hydrate and capillary pores). The distinction is made on the basis of NMR T_2 relaxometry, [22]. We label these fractions $\phi_{\rm il}$, $\phi_{\rm gel}$ and $\phi_{\rm cap}$ respectively noting that in what follows pores of inter hydrate size ("*ih*"; $\approx$ 20 nm) are considerably more important in the analysis than large (μm) capillary pores but that "*il*" and "*cap*" are more easily distinguished than "*il*" and "*ih*". We return to discuss this distinction later. A different transport coefficient is ascribed to each of these three porosity types. Hence we write

$$\frac{1}{D_{\rm eff}(\phi)} = \frac{\phi_{\rm il}}{D_{\rm il}} + \frac{\phi_{\rm gel}}{D_{\rm gel}} + \frac{\phi_{\rm cap}}{D_{\rm cap}}. \tag{4}$$

Recognise that in the absence of physical swelling,

$$\phi_{\rm il} + \phi_{\rm gel} + \phi_{\rm cap} = 1. \tag{5}$$

As written, this effective coefficient is a function of the pore size distribution but not of the water saturation within it. However, NMR results published previously [14] show that the pore size distribution depends on the *history* of the water saturation, so that $\phi_{\rm i} = \phi_{\rm i}(s,t)$ where $i =\in [il, gel, cap]$.

The innovative step within this work is to argue that the porosity composed of pores of different size is always relaxing towards a water saturation dependent equilibrium, $\phi_{\rm i}^0$, with a time constant $\tau_{\rm i}$ according to

$$\frac{\partial \phi_{\rm i}}{\partial t} = \frac{\phi_{\rm i}^0 - \phi_{\rm i}}{\tau_{\rm i}} \tag{6}$$

subject to the constraint Eq. 5. The constraint is accommodated by allowing the inter-layer and gel porosity to relax exponentially while equating the remaining porosity to the larger capillary sized spaces. Hence only two time constants, $\tau_{\rm il}$ and $\tau_{\rm gel}$ are introduced.

In total, Eqns. 2 to 6 provide a set of equations that can be parametrised from experiment and solved numerically subject to a set of boundary conditions. The idea of pore collapse is not new but hitherto there are only a few attempts to quantify it [14] [23] [24]. To help move towards further quantification, consider Fig. 1 which provides justification for how we parametrise the saturation dependence of the equilibrium porosity fractions. The figure shows schematically how, during a sorption cycle, pores empty and refill.

The concentration dependencies of the equilibrium pore fractions used in what follows result from the argument presented in the extended caption to Fig. 1. They are shown in Fig. 2 for both sorption and desorption. Irreversible changes associated with the first sorption cycle are not considered: all data presented in this work is for 2nd or 3rd cycle. At $s = 1$, and in equilibrium (*i.e.* after a sufficiently long time) the majority of the porosity is in pores of gel size, followed by inter-layer space size and lastly capillary pore size: $\phi^0_{\rm gel}(s = 1) > \phi^0_{\rm il}(s = 1) > \phi^0_{\rm cap}(s = 1)$. These fractions can be measured directly from the NMR T_2 distribution of a saturated sample. Muller *et. al* [25] previously measured the pore size resolved desorption isotherm for a similar cement as used here, albeit for first cycle. Further data for sorption can be found in the thesis of Gajewicz [26]. These works provide a lower bound on the equilibrium porosity fractions as they only measure filled pores. Notwithstanding they do reveal a good estimate for the saturation at which gel pores empty, $s_{\rm b}$, and also the enhancement of the inter-layer fraction, $\phi^0_{\rm il}(s = s_{\rm c}) - \phi^0_{\rm il}(s = 1)$ on the assumption that true inter-layer spaces remain full at saturation $s_{\rm b}$. We further assume that the gel pores do not collapse at saturations above $s_{\rm c}$ so that $\phi^0_{\rm il}(s = s_{\rm c}) + \phi^0_{\rm gel}(s = s_{\rm c}) = \phi^0_{\rm il}(s = 1) + \phi^0_{\rm gel}(s =$

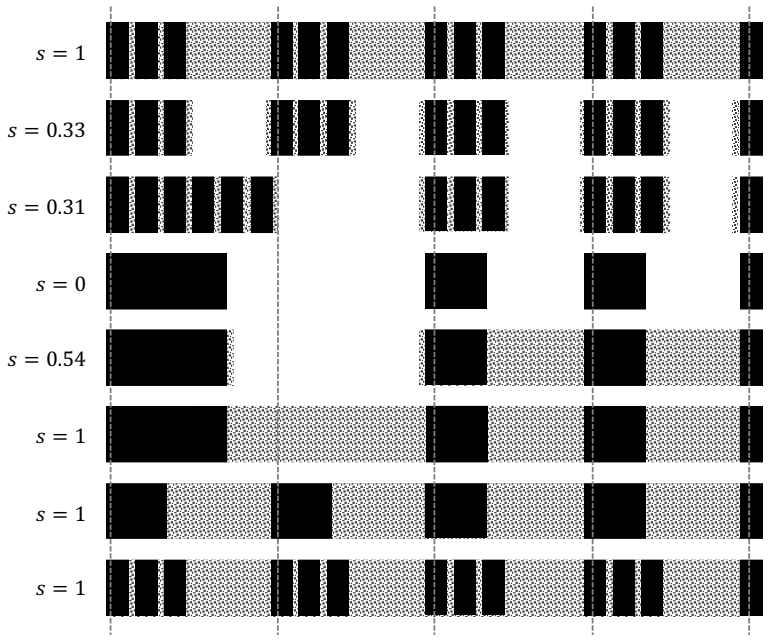

Figure 1: The figure shows a stylised section through C-S-H layers and gel pores during a sorption cycle. Although the cement is obviously amorphous, the cut shows a four times repeating sequence of three CaO backbones (solid black) with two inter-layers and one gel pore. The figure as drawn has a gel pore width about 10 times the size of an inter-layer space and a gel porosity about 5 times that of the inter-layer space both 2 to 3 times reality to ease visualisation. The vertical grey dotted lines mark the repeats. From top, initially, at $s = 1$, water (dot pattern) fills the inter-layer spaces between the backbones and the gel pores. During desorption, water is removed initially from the gel pores but leaves a residual surface layer that, from the NMR perspective, now manifests as inter-layer water. The apparent number of inter-layers increases. As drawn, this occurs at $s = 0.33$ and is where the apparent inter-layer population is a maximum. Continued drying causes some gel pores to collapse. As drawn, half collapse leading to the situation shown at $s = 0.31$. The number of apparent inter-layers is marginally reduced from its maximum. Yet further drying collapses the inter-layers, $s = 0$. If the system is refilled with water, then gel size pores refill first and other surface layers develop, as stylised at $s = 0.54$, 4th row from bottom. Larger pores then fill. Left alone, the gel and inter-layer pores relax back to the initial state on two timescales: first the gel sized pores and then the inter-layers, bottom two rows. The 2nd and 3rd rows correspond respectively to the situation at s_{c} and s_{b} as used in the text while s_{a} is the drying condition reached anywhere between the 3rd and 4th rows. Drying shrinkage is omitted from this discussion.

1).

The parameter that is most difficult to estimate is the fraction of gel pores that collapse. An indicative value will come from visual inspection of the data to be presented: a more refined value is available from data fitting and will be supported by an experiment involving n-decane. At $s = 0$ inter-layer spaces have collapsed as have a fraction of gel pores. All remaining porosity is of capillary pore size. We assume linear variation of the equilibrium pore size fractions between the fixed points. For sorption, consider a sample dried to $s_\mathrm{a} < s_\mathrm{b}$. Based on Fig. 1 we assume that the equilibrium pore fractions vary linearly with increasing s so as to return the staring point at $s = 1$. In summary then, parameterisation of the model equilibrium pore fractions only requires fixing of 7 numbers $\phi^0_{\mathrm{il,gel}}(s = 1)$, $\phi^0_{\mathrm{il,gel}}(s = s_\mathrm{b})$, $\phi^0_{\mathrm{il}}(s = s_\mathrm{c})$, s_c and s_b all as identified in the figure. This seems a lot. However, a large fraction can be measured directly from data published here or previously and good estimates can be made of the remainder.

If the transport mechanism is capillary driven, a simple scaling argument derived from the Lucas-Washburn equation suggests that, under conditions of total overall porosity, the capillary diffusivity of material comprising capillaries of size r scales as

$$D \propto \frac{1}{r}. \tag{7}$$

NMR evidence from different sources suggests that the pore widths for cement gel, ($r_\mathrm{il}, r_\mathrm{gel}$ and r_cap), scale approximately as 1:3:9 leading to

$$\frac{1}{D(s)} = \frac{1}{D_\mathrm{il}} \left(\frac{\phi_\mathrm{il}}{1} + \frac{\phi_\mathrm{gel}}{3} + \frac{\phi_\mathrm{cap}}{9} \right). \tag{8}$$

To restrict the number of fitting parameters in what follows, we find that we are able to fix the ratios between the 3 diffusivities in this way, save

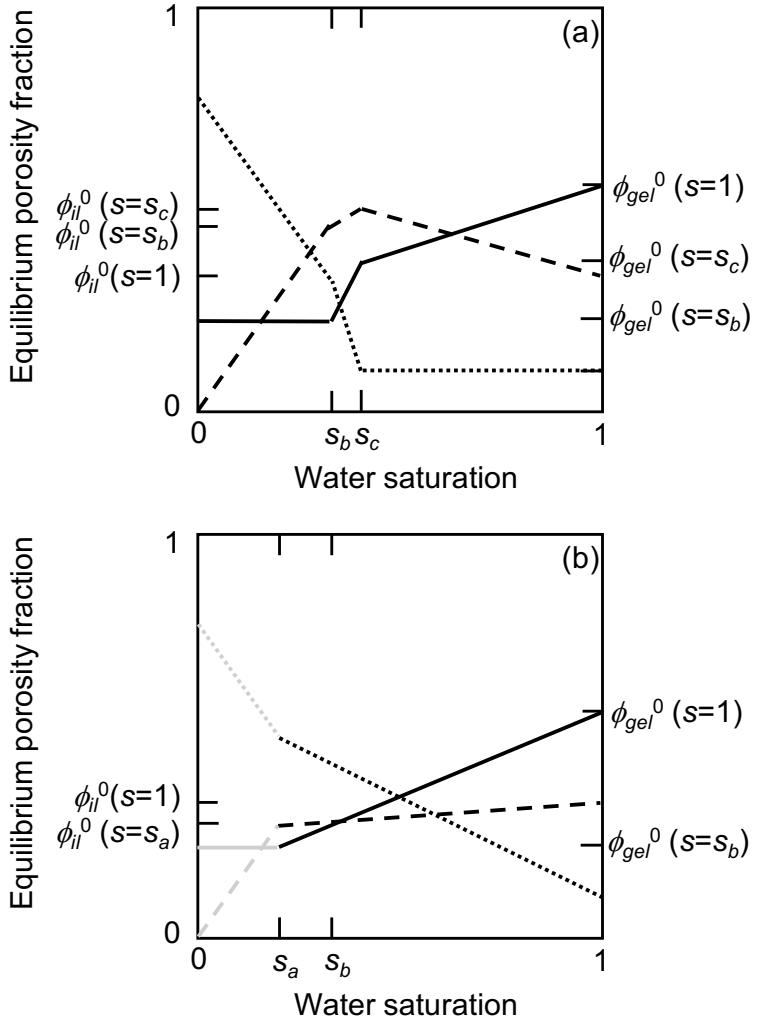

Figure 2: (a) The figure shows the (assumed linear) dependences of the equilibrium porosity fractions during desorption for the inter-layer space (dashed line), and the gel (solid line) and capillary (dotted line) pores above, between and below the critical saturations, $s_{\rm c}$ and $s_{\rm b}$ at which the apparent inter-layer porosity reaches a maximum and the gel pores empty respectively. This representation quantifies the concepts of Figure 1. The capillary porosity is given by $s_{\rm cap} = 1 - (s_{\rm gel} + s_{\rm il})$ and is assumed constant for $s > s_{\rm c}$. The lines are fully defined by inter-layer and gel porosities defined in the figure and described in the text. Most of these numbers can be measured directly from NMR data. (b) The equilibrium pore fractions during sorption for a sample pre-dried to $s_{\rm a}$. The grey lines carry over from the desorption isotherm meaning that no additional parametrisation is required.

that a larger multiplicative factor is required. One reason may be that in very small spaces structuring of water around dissolved ions and near double electric layers at surfaces greatly hinders transport.

3. Materials and methods

3.1. Materials

The white cement used had a composition C_3S 77 %, C_2S 16 %, C_3A 5 % and C_4AF 1 % as reported by the manufacturer. Batches of 80 g cement were mixed with distilled water in the mass ratio $w/c = 0.4$ for 2 min at 1600 rev/min. The paste was then further mixed for 1 min at 320 rev/min in a vacuum mixer. The paste was cast in cylindrical moulds 100 mm long and 15 mm in diameter. The moulds were sealed until the paste was set sufficient for the cylinders to be removed and cured under $Ca(OH)_2$ solution for a minimum of 28 days. The cylinders were then sliced into circular discs 15 mm diameter and 1 to 1.5 mm thick, ensuring parallel sides. The cutting was done with a diamond saw at 0.9 mm/min. The slices were further stored in $Ca(OH)_2$ solution until required.

Prior to NMR measurements, samples were taken through 2, $2\frac{1}{2}$ or 3 sorption cycles. Drying was carried out at 60 °C in a vacuum oven for 24 hrs. Re-wetting was accomplished by submersing the samples in $Ca(OH)_2$ solution for 24 hours. No samples were measured after a single cycle to ensure that irreversible effects associated with that cycle were excluded from the analyses.

3.2. Spatially selective magnetic resonance

^{1}H NMR measurements were made using a GARField design magnet [27] operating at approximately 20 MHz. Fig. 3 shows a schematic of the set up. The GARField used incorporates a strong permanent magnetic field gradient of 9.16 T/m in the vertical direction so that the exact resonance frequency depends on depth into the sample with a rate of change of 390 Hz/μm. A probe was specially built to house and level a disc of cement paste 15 mm in diameter and up to 1.5 mm thick. The probe sealed around the circumferential edges of the sample. The probe was fitted with a Helmholtz-like pair of dual RF transmit / receive NMR coils of 5 mm diameter placed above and below the sample. This configuration ensured more uniform NMR signal excitation and detection through the depth of the sample. The small diameter of the coils ensured that signal was only detected from the central region of the circular disc, avoiding any potential circumferential edge effects. By varying the frequency, the depth of the region within the sample was chosen.

Four small holes in the probe, one above, one below and two to the side of the sample allowed the ingress and egress of either water or vapour. For wetting studies, a dried sample was placed in the magnet. A pre-wetting NMR measurement was made. The top hole was used to place a small volume (typically 50-60 μL) of water on the upper sample surface. NMR measurements were made throughout the wetting period, initially at about 4 minute intervals, more slowly as the experiment progressed to allow more averaging and better signal-to-noise ratio. Note, however, that multiple depths were examined, so data sets were not necessarily recorded at this rate at a single

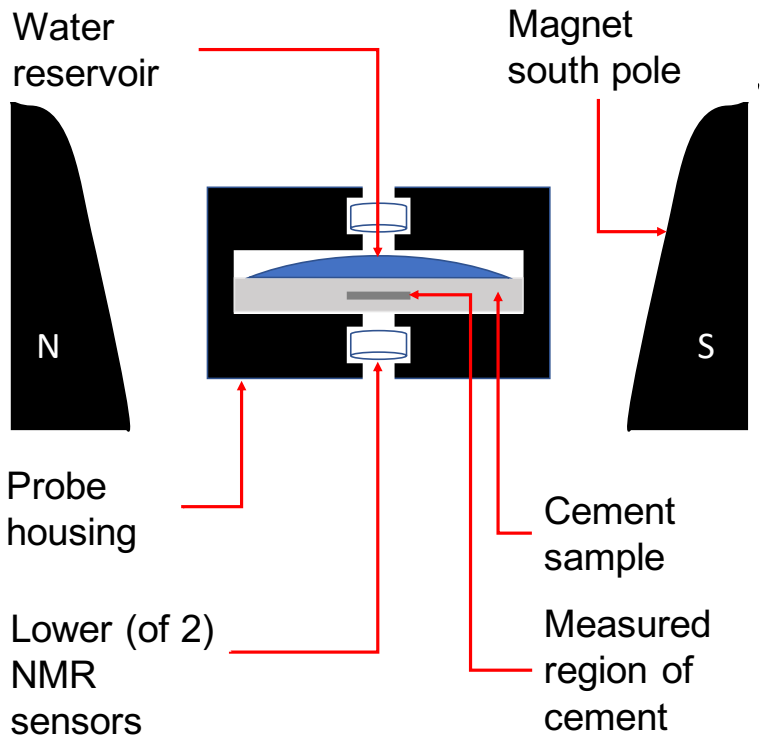

Figure 3: A schematic of the GARField magnet and probe as set up for a sorption experiment. The magnet north and south pole pieces are shown to the left and right. The probe casing (centre, in black) houses a cement disc (grey) and two NMR sensors (small coils of wire). The measured central slice of the cement disc is shown in darker grey. The cement disc is 15 mm diameter, 1.5 mm thick. Water (50-60 μL, blue) is placed on the upper surface of the sample through the top hole.

depth throughout. The lower hole was left open to allow air egress from below. The surface water was visible in the MRI and this facilitated periodic top-up of the level. The pre-wetting MRI measurement was additionally used to locate the sample surface, to ensure that the sample was mounted level and to calibrate the measurement depth. For drying, an initially saturated

sample was positioned in the magnet. A gentle air stream (60 L/hr) was passed through a large volume of dry silica gel and then onto the sample top surface though the top hole, exiting a side hole. Again periodic NMR measurements were made.

For the NMR, the quadrature echo train sequence was used. This is defined, in standard notation, by $P_{\mathrm{x}}^{90} - \tau_{\mathrm{NMR}} - \left(P_{\mathrm{y}}^{90} - 2\tau_{\mathrm{NMR}} -\right)_{\mathrm{n}}$ where it is understood that the pulse length is set at the slice centre frequency [28]. NMR echoes were acquired during each of the $n = 64$ $2\tau_{\mathrm{NMR}}$ windows (16 data points at a sampling rate of 1 MHz). The exact NMR frequency was adjusted so that the resonance condition occurred at a depth of (normally) 600 μm in the sample. A value of $\tau_{\mathrm{NMR}} = 20$ μs was used throughout so that the echo time spacing was $\tau_{\mathrm{echo}} = 40$ μs. The pulse length was circa 2 μs in length, corresponding to a bandwidth of circa 500 kHz and a useful spatial field of view of about 1300 μm. The data sampling of 16 points at 1 MHz gives a spatial resolution of circa 160 μm within that field of view. The repetition time was typically set at 0.1 s so that 2048 averages required about $3\frac{1}{2}$ min.

3.3. Data Analysis

The GARField data analysis comprises four steps.

First, it is well known that the first echoes of the quadrature sequence weakly oscillate if the pulse is not perfectly set (which it never can be across the whole sample depth due to the magnetic field gradient). Also the first echo is systematically attenuated, [29][30]. For these reasons, all echo intensities were corrected by the signal from a spatially uniform, homogeneous rubber test sample.

Second, the echo encompasses signal from across a slice of finite width dictated by the magnetic field gradient strength and pulse length. In order to measure at the prescribed depth, every echo was sine-bell filtered and Fourier transformed. Then the absolute value of the signal intensity at the centre of the transformed spectrum was recorded. The spectrometer bandwidth attenuates the signal in the wings of the spectrum. Notwithstanding, intensity in the wings of the spectrum is sufficient to recognise the sample surface and to check the accurate sample positioning. Taking the absolute signal leads to problems with baseline offset for low amplitude, slowly decaying components. However, this was considered a more minor problem compared to phasing GARField data.

Third, the necessarily short echo time leads to some of the crystalline solid ($Ca(OH)_2$, ettringite *etc.*) signal coming through into the echo train decay. This was subtracted out as follows. In order to measure the "solid" contribution, a regular homogeneous magnetic field bench top experiment was carried out on equivalent cement samples before the experiment using the more common single quadrature echo sequence. The two pulses and echo of this sequence are identical to the start of the multiple quadrature echo sequence used in this work with GARField. The single echo sequence with variable τ_{echo} is used to differentiate evaporable and "solid" water. Hence the solid fraction in the first echo of the GARField experiment is found. Oven dried, analytical grade, $Ca(OH)_2$ was also measured in the homogeneous magnet using the multiple echo sequence with with $\tau_{\text{echo}} = 40\mu$s to get the best estimate possible for the decay curve for the "solid" in GARField. Then, thereby knowing the "solid" signal fraction in the first echo and the solid

decay shape, the contribution due to crystalline solid was subtracted from all the GARField echo trains recorded. The key assumptions are that decay of $Ca(OH)_2$ is sufficiently representative of all the "solid" in the cement and that the amount of "solid" is independent of the degree of water saturation. It was checked experimentally that the shape of the decay curve in the homogeneous field was the same as in GARField. The former was used simply because it had a far superior signal-to-noise ratio.

Fourth, the remaining echo train intensity data was fit to a multi- exponential decay curve. Although good, the data was of insufficient signal-to-noise ratio to enable T_2 fitting by inverse Laplace transformation. Rather, on the basis of previously published work, the decays were fit to a 3 component exponential decay with constrained T_2 decay times using a least squares algorithm. The T_2 values were chosen by careful analysis of hydrated samples and by comparison with earlier work using homogeneous magnetic field NMR on similar cements. The T_2 values were considered constants throughout the experiments. This methodology ignores gradual changes resultant from gradual changes in pore sizes but does satisfactorily assign intensities to the three (water filled) pore size fractions.

3.4. Numerical Methods

A finite difference MATLAB® script was written to numerically solve equations Eqns. 2 to 6 in one dimension starting from an initial condition of either a uniformly saturated or dried matrix. The solution was found for a pre-defined set of equilibrium porosity functions. The boundary condition at the open end of the matrix ($x = 0$) was either a constant surface saturation ($s(x = 0) = const.$) or a constant drying rate ($\partial s/\partial t|_{x=0} = const.$). A no-

flux boundary condition was imposed at the closed end, ($\partial s/\partial t|_{x=x_{xmax}} = 0$). The equations were solved through iterative steps of advancing the transport (Eqn. 2) and relaxation (Eqn. 6) equations.

The method of steepest descent was used to fit the model to the data. The transport-relaxation equations were solved for a system with length equivalent to the sample thickness, initial and boundary conditions appropriate to the experiment and a starting test set of parameters $p = [D_{\mathrm{il}}, D_{\mathrm{gel}}, D_{\mathrm{cap}}, \tau_{\mathrm{il}}, \tau_{\mathrm{gel}}]$. The three saturation levels as a function of time, $s_{\mathrm{i}}(t)$, were output for $x = x_{\mathrm{NMR}}$ and the data separately subtracted to find the residuals for each pore size. These were summed to find a global measure of the quality of the fit, R. Care was taken to sample the data uniformly in $t^{1/2}$ space to avoid overweighting data at the end of the experiment. The partial derivatives $\partial R/\partial p$ were calculated for the model parameters by sampling R in the immediate vicinity of the test parameters. The test parameters were moved in the direction of steepest decent of R in parameter space and the procedure iteratively repeated until the change in R per cycle was about 0.001 %. Each iteration required about 2-3 s CPU time running in MATLAB® and circa 50 to 100 cycles were required to find a minimum of R. By varying the starting parameters widely, and also by varying the more poorly defined parameters defining the equilibrium porosity functions $[\phi^0_{\mathrm{gel}}(s_{\mathrm{b}}), \phi^0_{\mathrm{il}}(s_{\mathrm{c}})]$, it was checked that the minimum found was a global minimum. The broad sensitivity of the model to different parameters was explored and an estimate of the uncertainty in the best fit parameters was determined.

Finite difference solution of the transport (diffusion) equation can be numerically unstable leading to erroneous results if the time step size is not

well matched to the diffusivity and space step size. This becomes an issue especially when the diffusivity is a strong function of the saturation. The relaxation step as introduced here imposes an additional complexity. To ensure that the numerical results were accurate and not subject to artefact arising from the numerical methodology, a Monte Carlo code was also written to solve the same equations. The results were essentially the same for similarly parametrised simulations.

4. Experimental results and analysis

4.1. Sorption by a dried sample

We consider first a cement paste sample that was mixed, cast, cured underwater for 28 days and sliced as described in Section 3. The sample was then taken through three cycles of drying at 60 °C and wetting in a bath of calcium hydroxide solution prior to NMR measurements in order to eliminate any response associated solely with the first sorption cycle. Given the small size of the sample, there was no evidence of cracking as is routinely seen if a sample is dried at this temperature. NMR measurements were conducted throughout the final re-wetting during which time the sample was wet from the upper side only in the magnet.

Figure 4 shows three exemplar plots of echo train intensity (after Fourier transform, section 3.3 step 1) measured at a depth of 600μm below the wetted surface. The chosen experiment times - dry sample, and after 1 and 48 hours of sorption - are significant in terms of the sorption progress as will be seen. Each echo train took 4 min. to acquire. As presented, the echo intensities have been corrected for the rubber standard as discussed in section 3.3 step 2.

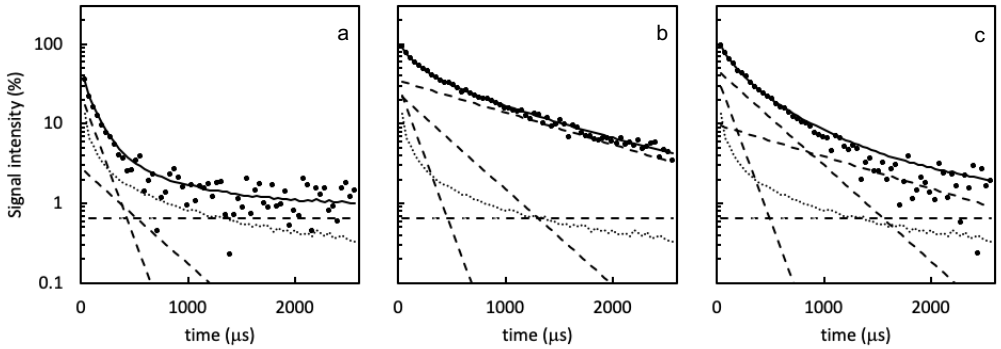

Figure 4: Quadrature echo train data for a sorption experiment for (a) dry sample and after (b) 1 hr and (c) 48 hrs sorption. The points are the experimental data corrected for the rubber standard. The solid line is the total fit. The dotted line is the (measured) contribution due to crystalline solids. The dashed lines are the three T_2 components with relaxation times of 120, 360 and 1080 μs and a baseline offset (0.7%). The data are scaled such that 100 % equates to the the total evaporable water signal (*i.e.* excluding crystalline solid) between 45 and 48 hrs of sorption. In (a) the longer T_2 component amplitude is less than the plot lower axis bound and hence not significant.

They are further normalised such that 100 % equates to the total evaporable water content averaged at the end of the experiment, between 45 and 48 hours. The solid line is the fit to the data. It comprises five parts shown by the other lines. The first (dotted line) is the measured contribution due to the (attenuated) crystalline solid, section 3.3 step 3, the evidence for which is presented in the next paragraph. The remaining three components (dashed lines) are the exponential decay fits to the data for which the T_2 relaxation times have been constrained to 120, 360 and 1080 μs respectively, section 3.3, step 4. A baseline offset of 0.7 % intensity is also included because the data is presented in magnitude mode format. In these examples, the evaporable

water fractions for the inter-layer, gel and capillary pore water are 24, 3 and 0 % respectively for the dry sample; 31, 24 and 35 % respectively after 1 hour sorption and 40, 48 and 10 % respectively after 48 hours sorption. Hence, after just 1 hour of sorption, the total measured evaporable water at a depth of 600μm is already 90 % of saturation at 2 days though the occupied pore size distribution is markedly different.

The crystalline solid signal subtraction shown in Fig. 4 is based upon the results presented in Fig. 5. The first part of this figure shows the results of the conventional homogeneous field quadrature single echo experiment on a similarly dried sample from which it is concluded that the ^{1}H crystalline solid and evaporable water signals are in the ratio 0.51 to 0.49. This is fully consistent with previously published work [31]. At $\tau_{\text{echo}} = 40$ μs the solid and liquid components are in the ratio 0.38 to 0.62. The second part of the figure shows the quadrature multiple echo train decay of dried $Ca(OH)_2$ recorded with an echo time of $\tau_{\text{echo}} = 40$ μs. Both bench top homogeneous field and GARField data are shown. They have the same shape though the bench top magnet offers far improved signal-to-noise ratio and does not suffer from the offset baseline of the GARField data. This bench top decay shape, at an intensity equivalent to 38 % of the first echo intensity of the dried sample, is subtracted from the recorded GARField echoes for all cement sorption GARField data.

Two validation checks are available. The first is to calculate the actual solid signal amplitude as a fraction of the total signal in the fully wetted sample. It is $(13.4 \times \frac{62}{38} \times \frac{51}{49})/(13.4 \times \frac{62}{38} \times \frac{51}{49} + 100) = 19\%$ where 13.4 % is the intensity of the first $Ca(OH)_2$ echo in Fig. 4. This is in general agreement

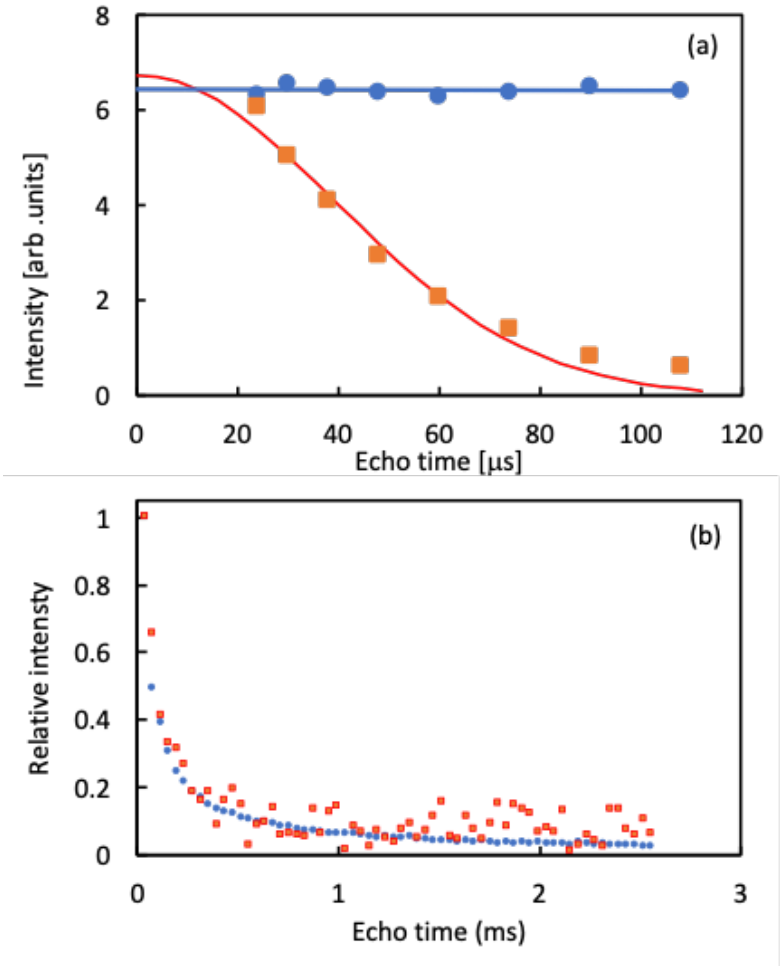

Figure 5: (a) The solid echo (red squares and Gaussian fit line) and liquid FID (blue circles and linear fit line) component intensities recorded as a function of echo time $\tau_{\text{echo}} = 2\tau_{\text{NMR}}$ in a bench top homogeneous magnetic field experiment for a cement paste sample dried at 60 °C. The solid to liquid ^{1}H content ratio is 0.51:0.49. For $\tau_{\text{echo}} = 40\mu$s, the apparent ratio is 0.38:0.62 (b) The multiple quadrature echo train intensity decay recorded with $\tau_{\text{echo}} = 40\mu$s for dried $Ca(OH)_2$ using a bench top (blue circles) and GARField (red squares) system.

with expectation for an as-prepared, never-dried, sample (24%), [22][25]. The second is to calculate the ratio of total pore water to inter-layer space water for the re-wetted sample. It is $(48 + 10) : 40 = 1.45 : 1$, less than previously $(2 : 1)$, but not wildly out of line and possibly explicable by the irreversible changes occurring on first desorption.

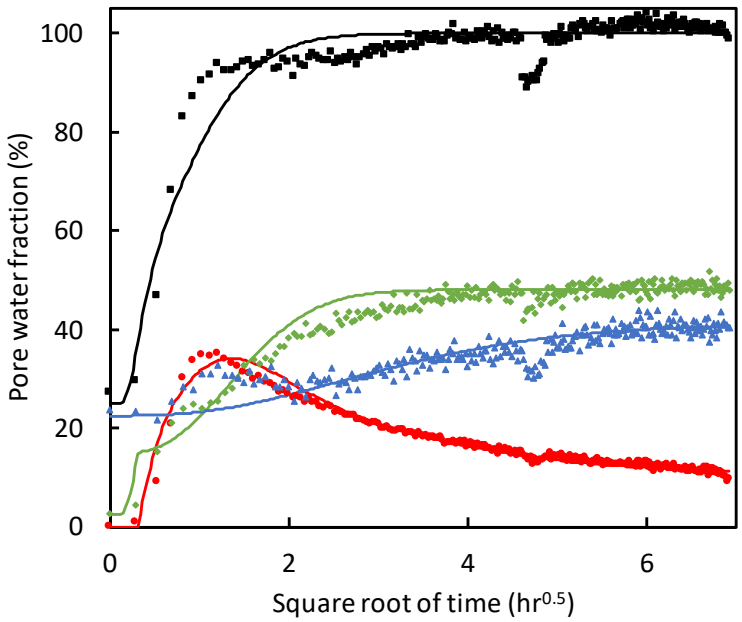

Figure 6: Filled porosity fractions measured 600μm below surface for the sorption experiment. The red circles are for water in capillary sized pores; green diamonds for gel sized pores; and blue triangles for inter-layer spaces. The black squares are the total and the solid lines are fits to the data using the model presented in Sec. 2.

Figure 6 shows the temporal dependence over 2 days of the evaporable water saturations by pore size as a function of the square root of the rewetting time. The amplitudes are normalised such that the mean total amplitude

recorded over the last 3 hours is 100 % indicating filled porosity although, of course, it is an assumption that the sample is fully saturated at this depth at this time. The data points at zero time were recorded prior to the commencement of the final wetting cycle, that is from the dried sample. The data show a short initial delay during which time the penetrating water front does not reach a depth of 600 μm. Thereafter there is a rapid rise in capillary water which, after about 1 hr, starts to fall away again. The gel pore water rise is rapid at first. It then slows before picking up once more reaching a plateau after approximately 16 hr. The inter-layer water increases gradually across the whole time period save that there is a small local maximum around 1 hour, possibly associated with the formation of surface water layers in gel pores before these fill fully. Notice that the total water saturation reaches 90 % of maximum very quickly. The changes in porosity fractions therefore primarily reflect a redistribution of porosity. The jump in the data around 25 hrs. occurred when the probe water reservoir was topped up. The features seen are generally reproducible across multiple samples.

4.2. Drying of a saturated sample

Figure 7 shows the pore water fractions at a depth of 600 μm below the surface of a nominally fully saturated sample during drying in the magnet. A gentle flow of dry air passes continuously over the upper surface of the sample. For the first approximately 1 hour, very little happens. The drying front does not extend down to 600μm. Thereafter, and for the duration of the experiment, the sample dries steadily. Total water loss at 600 μm varies approximately with $t^{1/2}$. Inspection of the water fraction in different pore sizes shows that the largest pores empty first, as expected. They have

emptied by 4 hours. From 4 hours until the experiment ends at 6.5 days there is a continuous decrease in the water fraction in gel pores that is faster than the total water loss. The difference is accounted for by an increase in the apparent inter-layer water fraction. Notice that the filled capillary pore fraction at the start of the experiment is rather low, about 8 %. It takes some minutes to load the sample into the cell during which time it is exposed to atmospheric conditions. The sample is very thin and we suspect that the very largest capillary pores arising from chemical shrinkage dry almost instantly whilst the sample is mounted in the probe and the probe is sealed and tuned. Hence, the intensities of all the signals have been renormalised such that, on the basis of matching to the end of the sorption experiment, the initial saturation is 93 %.

4.3. Validity of the observed changes in pore size distribution

It is hard to independently validate the highly localised changes in filled pore size distribution seen in the NMR studies. However, it has been reported that inorganic solvents such as isopropanol and n-decane ingress cement normally, that is as $t^{1/2}$ [32]. To that end, we have conducted sorption experiments analogous to that reported in Sec. 4.1 except that we have used these alternate invading fluids. Fig. 8 shows the results for n-decane. The results are substantially the same using isopropanol. The $Ca(OH)_2$ subtraction amount was adjusted so that the dry sample is equivalent to previously as we do not have a comparable bench top experiment for comparison. The data is fit to 3 T_2 components, 120 μs for the residual inter-layer water; 5000 μs for the gel water and a variable baseline (because the longest T_2 is too long to measure) for the capillary pore water. The huge increase in the last

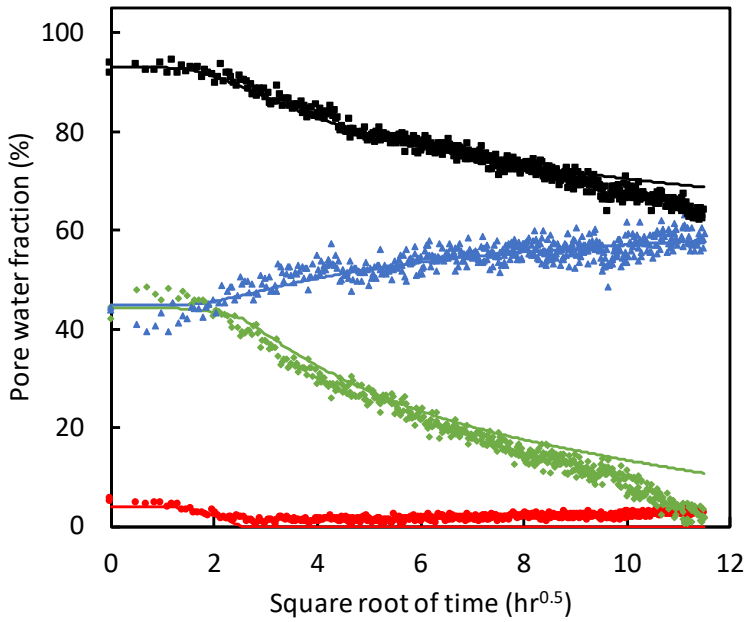

Figure 7: Filled porosity fractions measured 600μm below surface for the drying experiment. The red circles are for water in capillary sized pores; green diamonds for gel sized pores; and blue triangles for inter-layer spaces. The black squares are the total and the solid lines are fits to the data using the model presented in Sec. 2.

two relaxation times compared to the water experiments reflects the very different surface interaction of n-decane compared to water. It is not relaxed anywhere near as efficiently. What is immediately obvious is that there is a very clear wetting front that ingresses the sample. It arrives about 35 min. after the start of the experiment. Once the front passes, the filled pore size distribution remains constant. The fact that the amount of capillary size porosity far exceeds that of the gel pores suggests that most gel pores have collapsed. The n-decane has invaded the newly created larger porosity and

has stayed there in accordance with the drying, but not wetting, scenario presented in Figs. 1 and 2. We do not see the porosity changes seen with water on sorption. Although indirect, we suggest that this is very supportive of the link between dynamic porosity and anomalous transport.

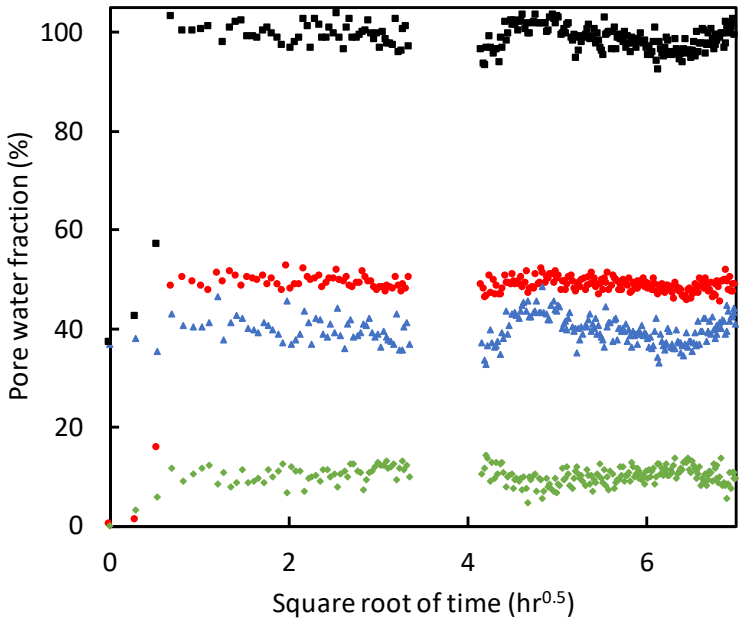

Figure 8: The results of a sorption experiment using n-decane as the invading fluid otherwise similar to that with water shown in Fig. 6. The red circles are for water in capillary sized pores; green diamonds for gel sized pores; and blue triangles for inter-layer spaces. Black squares are the total. A sharp ingress front is seen to arrive at 600μm after 0.6 hrs whereupon the cement rapidly saturates at this depth. Unlike with water, there are no subsequent changes in porosity. An unfortunate power outage meant that no data was recorded between about 10 and 16 hours into the experiment.

4.4. Numerical model: parametrisation and analysis

4.4.1. Equilibrium porosity fractions

Estimates for the parameters defined by Fig. 2 that define the equilibrium pore size distributions for sorption and desorption are determined directly from the data shown here and from the previously published pore size resolved sorption isotherm data (notwithstanding that earlier data is for a first sorption cycle). For the case of sorption, the porosity fractions for $s = 1$ are measured from the data at the end of the experiment. The degree of saturation at the start of wetting, ($s_{\mathrm{a}} = 0.27$) is determined by direct comparison of the total evaporable water signal at the start and end of the experiment as previously discussed. The division of the porosity at s_{a} depends on the saturation and porosity parameters s_{b} and $\phi^0_{\mathrm{gel}}(s_{\mathrm{b}})$. A good estimate of s_{b} corresponding to the 3rd row in Fig. 1 but based on the first sorption cycle [25] is $s_{\mathrm{b}} = 0.43$. Analysis here refines the value to $s_{\mathrm{b}} = 0.5$ for later cycles. The other, $\phi^0_{\mathrm{gel}}(s_{\mathrm{b}})$, is estimated to be 0.25 from the early step in the gel porosity signal seen in Fig. 6; however a more refined analysis of the desorption data reported below gives $\phi^0_{\mathrm{gel}}(s_{\mathrm{b}}) = 0.15$. For the case of desorption, many of these parameters can be similarly measured from the data. Some slightly different values (experimental variation) are found. However, to avoid "over fitting", we choose to leave all the above parameters unchanged as, logically, the end of desorption is the start of sorption and *vice-versa* beyond first cycle. Thus the only remaining unknowns are s_{c} and $\phi^0_{\mathrm{il}}(s_{\mathrm{c}})$. These are evaluated based on analysis of the desorption data and are found to be 0.65 and 0.6 respectively. A summary of all these values, and of those derived from them, are given in Table 1.

Saturation (dimensionless)	Equilibrium inter-layer porosity (%)	Equilibrium gel porosity (%)
$s = 1$	41	48
$s_c = 0.65$	60	29
$s_b = 0.50$	45	15
$s_a = 0.27$	24	15

Table 1: Parametrisation of the equilibrium pore size distribution functions defined in Fig. 2 and as used in this work. Note that $\phi^0_{il}(s_c) + \phi^0_{gel}(s_c) = \phi^0_{il}(1) + \phi^0_{gel}(1)$. Note also that s_a is the saturation to which the *sorption* experimental sample is pre-dried. The porosity fractions for s_a come directly from the *desorption* distribution and so are *not* independent parameters of the model.

4.4.2. Sorption

The solid lines in Fig. 6 are fits of the model to the data using the equilibrium porosity parameters from Table 1. The best fits have been identified using the steepest descent algorithm starting from a wide variety of starting positions in parameter space. The best fit parameters are listed in Table 2. The quoted uncertainties reflect the range of the parameters for which comparably good fits (measured by the sum of residuals varying by less than about 10 %) are achieved. There are five model model fitting parameters: three diffusivities and two time constants. These require some explanation and discussion.

Consider first the diffusivities. Inspection of Eq. 3 shows that the transport coefficient is dominated by the smallest diffusivity which is that for the inter-layer spaces. This is to be expected as the hydrate layers create low

Diffusivity	10^{-9} m^2/s	Relaxation time	hrs.
$D_{\rm il}$	0.05 ± 0.01	$\tau_{\rm il}$	12 ± 2
$D_{\rm gel}$	0.25 ± 0.10	$\tau_{\rm gel}$	1.7 ± 0.3
$D_{\rm cap}$	2.5 (not sensitive)		

Table 2: Best fit model parameters for water sorption analysis

permeability barriers between the (not connected) pores. The model fit is very insensitive to the diffusivity in capillary sized pores. Equally the model fit is not overly sensitive to the gel porosity diffusivity although changing it appreciably does vary the quality of fit. The fit of the effective diffusivity is most sensitive to the rate of rise of the first water observed at a depth of 600μm. Notice in the data that there is a delay of circa 20 min. or 1200 s before the water accumulates. Hence an estimate of the expected effective diffusivity at the start is $(600 \times 10^{-6})^2/1200/2 = 0.15 \times 10^{-9}$ m^2/s. The best fit parameters from the steepest decent multi-parameter fitting inserted into Eq. 3 yields 0.2×10^{-9} m^2/s at the start of the experiment in reasonable agreement. In the later stages of the experiment, the diffusivity reduces to just less than 0.10×10^{-9} m^2/s.

Consider next the relaxation times. An attempt was made to fit the data using just one relaxation time. This failed. The two parameters, $\tau_{\rm gel}$ and $\tau_{\rm il}$ are most sensitive to the rise of the gel porosity and inter-layer space water respectively. These occur somewhat independently and so both times can be well fit with reasonable precision and sensitivity. It is very clear that the inter-layers relax more slowly than the gel pores.

The fits are additionally sensitive to $\phi^0_{\rm gel}(s_{\rm b})$, the amount of gel pores

that do not collapse. If all gel pores collapse, then the model predicts that capillary pores initially fill and that there is a longer delay before water in gel porosity is seen - it has to recover first (apparently on a timescale of 1.7 hrs.). This is clearly contrary to the data. Gel pore water is seen before capillary water because there is residual gel porosity after drying and the smaller pores fill first. Careful inspection of the data shows a small step or pause in the rise of the gel signal. We believe (and this is consistent with the data) that this arises after the residual porosity first fills at 600 μm and before further gel porosity relaxes. The position of the step suggests that the residual gel porosity saturation is about 0.25. However, the fitting finds lowest residuals for 0.15 as used and listed in Table 1. There is also the noticeable local maximum in the apparent inter-layer space water signal occuring at about the same time. We believe that it is due to surface water layers forming in gel pores just before they fill fully. The model does not capture this well. One reason may be that we have used an overly simple parametrisation of the equilibrium porosity functions using straight lines to capture what is likely to be a complex equilibrium porosity function. Finally, we note that the validity of the residual gel porosity of about 15 % is supported by the n-decane data. The filled gel pore fraction, after wetting with n-decane in Fig. 8 is about 12-15 %.

4.4.3. Desorption

The solid lines in Fig. 7 are fits of the model to the data. The fits are made using the same parametrisation of the equilibrium porosity fractions as for the sorption experiment in order to reduce the number of fitting parameters save that an additional parameter pair, not required for sorption,

is needed: s_c and $\phi_{il}^0(s_c)$ are required. Inspection of the data, and the subsequent fitting suggest 0.65 and 0.60 respectively as listed in Table 1. The drying surface boundary condition also needs to be defined. The measured relative humidity of the drying air at source is nominally 10%. On the basis of a constant drying surface saturation this corresponds to an evaporable water saturation of $s(x = 0) = 0.45$ $t \geq 0$, [25]. However, we cannot make good fits to the data for this value and suspect that it is actually rather higher corresponding to $s(x = 0) = 0.6$. The most likely explanation is the relatively slow flow of air through the probe system and consequent opportunity for back diffusion of water vapour into the probe. Another is that the drying silica gel progressively wets during the course of the experiment (6 days). We note here that good fits cannot be made for a constant surface evaporation flux as might otherwise be used. Hence we conclude that drying is water diffusion (in the sample, to the surface) limited As with sorption, the dominant diffusivity is that for the inter-layer porosity. The best fits are found using $D_{il} = 1.3 \times 10^{-12}$ m^2/s. This is very much smaller than before. However, the driving force for drying is expected to be very much weaker, so this is not surprising. The fits are not especially sensitive to the other two diffusivities so long as they are sufficiently large by comparison. The ratios are kept as before so that $D_{gel} = 6.5 \times 10^{-12}$ m^2/s and $D_{cap} = 65 \times 10^{-12}$ m^2/s. Finally, and notwithstanding the self-evident growth of the inter-layer signal with drying, the relaxation time constants for best fit of the data are short. Indeed, the relaxations could be *quasi* instantaneous. However, all we can say is that both τ_{il} and τ_{il} are less than a few minutes which is the temporal resolution of the early data. Hence, for this *slow* drying, the porosity

relaxation is not a cause of anomalous drying and none is seen. The actual fits shown are made with $\tau_{\rm il}^{\rm desorp} = \tau_{\rm gel}^{\rm desorp} = 0.15$ hr. This is discussed further in the next section.

5. Discussion

In this section we reflect on different aspects of the forgoing analysis.

- Multi-parametric fitting.

A criticism of many multi-parameter models is that the best fit parameters are inter-dependent. As a result, they can be strongly correlated and do not permit robust data fitting. Consider first the equilibrium pore size distributions. Parameters that are associated with filled pores can be, in principle unambiguously, read from the data. The subset that cannot is relatively small and pertain to different parts of the sorption / desorption curves so are relatively independent. Hence we do find a problem here. Notwithstanding, in the future, since it appears that organic solvents do not change the pore size distribution in the way that water does, it may prove possible to measure equilibrium pore size distributions directly by first drying samples very slowly to a controlled relative humidity and then refilling the porosity with solvent and measuring the total distribution, water plus solvent. This procedure could replace the"straight-line" approximations by measured curves.

Consider next the dynamic parameters. The fitting is mainly sensitive to three only, the inter-layer diffusivity and the two relaxation times. Each is sensitive to different features in the data. As a result, a strong correlation between pairs of parameters arising from different estimates of the best fit is not expected, and none was found.

Another issue is the multi-component T_2 fitting. This is notoriously difficult as it is an ill posed problem. However, we are confident that the methodology we have adopted is not giving rise to artefacts that impact the results in any meaningful way. We have explored an alternate exponential fitting method, exponential stripping, and also varying the relaxation times. The former gives very similar results; the latter does not produce consistently good fits across the board.

- Cement sorptivity and capillary diffusivity.

Compared to mortars and concretes, there is relatively little water sorption and capillary diffusion data published for cement pastes. Amongst the limited data available, Casnedi *et. al* [33] report a sorptivity value of 0.9 $\mathrm{mg/cm^2/s^{0.5}}$ for an air dried Portland cement cube with $w/c = 0.43$. This approximates to a capillary diffusivity of 0.085×10^{-9} $\mathrm{m^2/s}$. This is satisfyingly comparable to the value of $D_{\mathrm{eff}} = 0.1 \times 10^{-9}$ $\mathrm{m^2/s}$ found in the later stages of our experiments, this late stage comparison being made remembering that an air dried sample is less severely dried than an oven dried sample. Ceballos-Ruano *et. al* [34] report diffusivity values of about 0.05×10^{-9} $\mathrm{m^2/s}$. However, this is on the basis of NMR measurements of (normal H_2O) water into D_2O saturated cement paste samples and *vice-versa*. Hence this is effectively a measurement of self-diffusivity, not capillary diffusivity, and is expected to be smaller than measured in this work. Yamaguchi *et. al* [35] report comparably small values for the similar (self) diffusion of tritiated water through H_2O saturated samples.

- Relaxation time constants different for sorption and desorption.

The data presented here has made evident that the porosity relaxation time constants on wetting are much longer than on drying. We suggest the reason for this is that, on wetting, water is already filling the porosity that requires to relax. In consequence water needs to migrate around the hydrate layers in parallel with relaxation. This takes time. On drying, the reverse is true. The water is already removed so no water rearrangement is required and the structure can relax more easily. It is interesting to note the the two relaxation times found for sorption are in general accord with the typical time for crossover between different rates of sorption commonly found in studies revealing anomalous sorption [9].

- Micro-cracking.

Cutting a cement paste sample, and then drying it at 60 °C undoubtedly introduces micro-cracks that affect transport. There is little that can be done here but in mitigation we note first that the samples are small, just 1.5 mm thick. There is no visually obvious micro-cracking as is seen when larger samples of say 5 cm size, are similarly dried. Second, the cracks as must exist do not form a connected network so transport must still proceed by passing through the hydrate gel. Third, the porosity changes that are a key aspect of this work are not affected by cracking. Finally, we note that if surface micro-cracking were significant, then it is unlikely that such a slow initial diffusivity would have been seen.

- Relationship to time dependent permeability models.

We compare the results of our model to Hall's very recent introduction of a locally time dependent permeability. Figure 9 shows the simulated mass

uptake over the first 100 hrs of sorption for a sample 50 mm long. This is sufficiently long that the sorption front does not appreciably reach the other end of the sample: $s < 4\%$ at the dry end for $t < 100$ hrs. It is evaluated using the same parameters as found from fitting the sorption experiment, Section 4.4.2, save that $D_{\text{cap}} = D_{\text{gel}} = 1.15\times^{-9}$ m^2/s. This single change to parameters to which our model is not very sensitive is made to tie in with Hall: the diffusivity at $s = 1$ is now 10 times that at $s = 0$ assuming equilibrated porosity in both cases: $D_{\text{eff}}(s = 1) = 1.15\times^{-9}$ m^2/s; $D_{\text{eff}}(s = 0) = 0.115\times^{-9}$ m^2/s. A distinct change of gradient in mass uptake is seen indicating sorption simulated on two timescales. The red dotted lines in the figure show the mass uptake for these two diffusivity values used as *constant* diffusivities. It is seen that they are the limiting rates in the short and long timescales. The form of the curve is very similar (but not identical) to that shown in Fig. 1 of Hall's work where there is also a ratio of 10 in the transport coefficient. That the shape of the curves are similar (but not exactly the same) is not surprising. The transport coefficient in Hall's model is derived from a permeability that locally starts to exponentially relax with a single relaxation time towards an equilibrium once a sharp wetting front arrives at any given point in the sample. The key advance in our work is the microscopic evidence for the detailed description of the relaxation, which, in fact, leads us to believe that in cement pastes there are at least two relaxation processes in play. Moreover, we do not need to invoke a sharp front and do explain differences between wetting and drying.

- Relationship to swelling models.

The key idea introduced by Alderete and co-workers is that water first in-

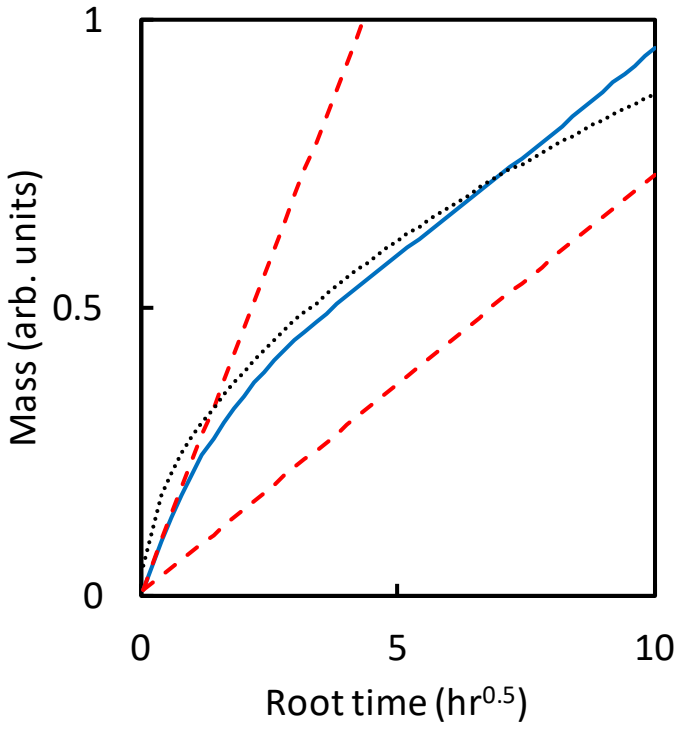

Figure 9: Simulated mass uptake into a sample designed to mimic the result of Hall based on a time dependent permeability. This figure should be compared to Figure 1 in reference [17]. The solid blue line results from the model presented in this work. The two dashed red lines are for constant effective diffusivity with equilibrium porosity evaluated at $s = 0$ and $s = 1$. The dotted line is $\propto t^{1/4}$ as advanced in [10]

vades the larger pores and then more slowly migrates into the finer porosity leading to a $t^{1/4}$ time dependency. We cannot disprove this idea but note that under some parameterisations, and over appropriate timescales, the new model leads to a behaviour that can look very much like $t^{1/4}$. For example, Figure 9 includes a dotted curve that is a $t^{1/4}$ fit to our own simulated data for a 50 mm sample that is itself a broad reproduction of the model described

by Hall (previous bullet). Differentiating between the models is difficult, but the current work provides experimental evidence over and above that which has previously been available in favour of a model based on a time dependent transport coefficient. However, we acknowledge that Alderete *et. al* also has supportive experimental data for mortars in the form of careful strain measurements.

- Drying shrinkage and swelling.

Swelling is excluded from the current analysis but does of course take place and in the context of anomalous transport is evidenced by the careful strain measurements by Alderete *et. al* just noted. Careful examination of Fig. 6 does show a gradual rise in adsorbed water of about 5 % occurring between about 4 and 48 hours of sorption. An evaporable water content of 5 % is equivalent to about 2.7 % of the cement paste volume and hence a length change of about 0.9 %. This figure is broadly consistent with short term drying shrinkage strains reported over timescales of a few hours by Maruyama *et. al* [16]. Hence, macroscopic swelling remains an additional mechanism not considered here. We do not think, however, that it is the dominant mechanism. Microscopic rearrangement of porosity at constant overall porosity, as here proposed, seems more important.

- Sorption isotherm measurements.

Many authors have reported measurements of sorption isotherms in cement pastes in which the change in sample mass is recorded over a very wide range of relative humidity. Since these experiments are generally of long duration, and since the total porosity (excluding discussion of shrinkage as

above) appears to be conserved, it is unlikely that the changes in porosity seen here will affect the measurement of absolute mass absorbed. However, the changes in porosity are likely to have an effect in experiments that seek to track mass changes occurring in loops where a sample is transitioned from one branch (say desorption) to the other (sorption) at intermediate relative humidities. The path taken could well depend upon the timescale of the changing environment. The timescale of the experiment is also likely to be an issue in experiments where pore size distribution is measured by, say N_2 sorption, in parallel with the mass loss isotherm measurement.

6. Conclusion

The first experimental evidence has been presented in which it is shown that changes in pore size distribution as a result of sorption into a previously dried cement paste sample that is rewet and that occur on a timescale of 1-15 hours offer a quantitive explanation of anomalous water sorption by capillary action occurring on a similar or faster timescale. Similar pore size distribution changes are seen in the case of sample drying. However, in the studies reported here the drying has been too slow to see reveal anomalies in desorption. It remains unclear whether (but it is unlikely that) the effects discussed here are sufficient to explain *all* cases of anomalous transport in cements but there is sufficient evidence to suggest that slow pore size changes are a significant contributing factor that should be taken more into account. The work to date has focussed on de/sorption just a short distance into the sample in an effort to deliberately and separately resolve spatial and temporal effects. Studies using other variants of magnetic resonance imaging

suited to larger (6 cm) sized samples are in progress to validate the ideas at longer length scales. Results will be published elsewhere, but early results are encouraging.

7. Acknowledgements

This work has received funding from the European Union Horizon 2020 Research and Innovation Programme under the Marie Skłodowska-Curie Innovative Training Networks programme grant agreement No. 764691.

8. References

[1] N. S. Martys, C. F. Ferraris, Capillary transport in mortars and concrete, Cem. Conc. Res. 27 (1997) 747-760.

[2] C. Hall, Anomalous diffusion in unsaturated flow: Fact or fiction?, Cem. Conc. Res. 37 (2007) 378–385.

[3] M. Saeidpour, L. Wadsö, Evidence for anomalous water vapor sorption kinetics in cement based materials, Cem. Conc. Res. 70 (2015) 60–66.

[4] Z. Wu, H. S. Wong, C. Chen, N. R. Buenfeld, Anomalous water absorption in cement-based materials caused by drying shrinkage induced microcracks, Cem. Conc. Res. 115 (2019) 90–104.

[5] C. Hall, W. D. Hoff, Water Transport in Brick, Stone and Concrete - Christopher Hall, William D. Hoff - Google Books, 2009.

[6] H. Ranaivomanana, J. Verdier, A. Sellier, X. Bourbon, Toward a better comprehension and modeling of hysteresis cycles in the water sorption–desorption process for cement based materials, Cem. Conc. Res. 41 (2011) 817–827.

[7] A. J. Bohris, U. Goerke, P. J. McDonald, M. Mulheron, B. Newling, B. Le Page, A broad line NMR and MRI study of water and water transport in portland cement pastes, Magn. Reson. Imag. 16 (1998) 455–461.

[8] S. Zamani, Magnetic Resonance Imaging Characterisation of Water Transport in Cement-Based Materials, Ph.D. thesis, University of Surrey, 2013.

[9] S. Zhutovsky, R. Douglas Hooton, Role of sample conditioning in water absorption tests, Construction and Building Materials 215 (2019) 918–924.

[10] Y. A. Villagrán Zaccardi, N. M. Alderete, N. De Belie, Improved model for capillary absorption in cementitious materials: Progress over the fourth root of time, Cem. Conc. Res. 100 (2017) 153–165.

[11] N. M. Alderete, Y. A. Villagrán Zaccardi, N. De Belie, Physical evidence of swelling as the cause of anomalous capillary water uptake by cementitious materials, Cem. Conc. Res. 120 (2019) 256–266.

[12] L. Monteilhet, J. P. Korb, J. Mitchell, P. J. McDonald, Observation of exchange of micropore water in cement pastes by two-dimensional

T_2-T_2 nuclear magnetic resonance relaxometry, Phys. Rev. E 74 (2006) 061404.

[13] P. J. McDonald, J. P. Korb, J. Mitchell, L. Monteilhet, Surface relaxation and chemical exchange in hydrating cement pastes: A two-dimensional NMR relaxation study, Phys. Rev. E 72 (2005) 011409.

[14] A. M. Gajewicz-Jaromin, E. Gartner, K. Kang, P. J. McDonald, V. Yermakou, A 1H NMR relaxometry investigation of gel-pore drying shrinkage in cement pastes, Cem. Conc. Res. 86 (2016) 12–19.

[15] I. Maruyama, T. Ohkubo, T. Haji, R. Kurihara, Dynamic microstructural evolution of hardened cement paste during first drying monitored by 1H NMR relaxometry, Cem. Conc. Res. 122 (2019) 107–117.

[16] I. Maruyama, Y. Nishioka, G. Igarashi, K. Matsui, Microstructural and bulk property changes in hardened cement paste during the first drying process, Cem. Conc. Res. 58 (2014) 20–34.

[17] C. Hall, Capillary imbibition in cement-based materials with time-dependent permeability, Cem. Conc. Res. 124 (2019).

[18] D. A. Lockington, J.-Y. Parlange, Anomalous water absorption in porous materials, J. Phys. D: Appl. Phys. 36 (2003) 760–767.

[19] J. Crank, The Mathematics of Diffusion, Oxford University Press, 1956.

[20] M. Van Landeghem, J.-B. d'Espinose de Lacaillerie, B. Blümich, J. P. Korb, B. Bresson, The roles of hydration and evaporation during the

drying of a cement paste by localized NMR, Cem. Conc. Res. 48 (2013) 86–96.

[21] R. Schulte Holthausen, M. Raupach, Monitoring the internal swelling in cementitious mortars with single-sided 1 H nuclear magnetic resonance, Cem. Conc. Res. 111 (2018) 138–146.

[22] A. C. A. Muller, K. L. Scrivener, A. M. Gajewicz-Jaromin, P. J. McDonald, Densification of C–S–H Measured by 1H NMR Relaxometry, J. Phys. Chem. C 117 (2013) 403–412.

[23] C. Zhou, F. Ren, Z. Wang, W. Chen, W. Wang, Why permeability to water is anomalously lower than that to many other fluids for cement-based material?, Cem. Conc. Res. 100 (2017) 373–384.

[24] C. Zhou, F. Ren, Q. Zeng, L. Xiao, W. Wang, Pore-size resolved water vapor adsorption kinetics of white cement mortars as viewed from proton NMR relaxation, Cem. Conc. Res. 105 (2018) 31–43.

[25] A. C. A. Muller, K. L. Scrivener, A. M. Gajewicz-Jaromin, P. J. McDonald, Use of bench-top NMR to measure the density, composition and desorption isotherm of CSH in cement paste, Microporous and Mesoporous Materials 178 (2013) 99–103.

[26] A. M. Gajewicz-Jaromin, Characterisation of cement microstructure and pore-water interaction by 1H nuclear magnetic resonance relaxometry, Ph.D. thesis, University of Surrey, 2014.

[27] P. M. Glover, P. S. Aptaker, J. R. Bowler, E. Ciampi, P. J. McDonald,

A Novel High-Gradient Permanent Magnet for the Profiling of Planar Films and Coatings, J. Magn. Reson. 139 (1999) 90–97.

[28] P. J. McDonald, B. Newling, Stray field magnetic resonance imaging, Reports on Progress in Physics 61 (1998) 1441–1493.

[29] T. B. Benson, P. J. McDonald, Profile Amplitude Modulation in Stray-Field Magnetic-Resonance Imaging, J. Magn. Reson. A 112 (1995) 17–23.

[30] M. D. Hurlimann, D. D. Griffin, Spin Dynamics of Carr–Purcell–Meiboom–Gill-like Sequences in Grossly Inhomogeneous B0 and B1 Fields and Application to NMR Well Logging, J. Magn. Reson. 143 (2000) 120–135.

[31] P. J. McDonald, V. Rodin, A. Valori, Characterisation of intra- and inter-C–S–H gel pore water in white cement based on an analysis of NMR signal amplitudes as a function of water content, Cem. Conc. Res. 40 (2010) 1656–1663.

[32] S. C. Taylor, W. D. Hoff, M. A. Wilson, K. M. Green, Anomalous water transport properties of Portland and blended cement-based materials - Springer, J Mater Sci Lett 18 (1999) 1925–1927.

[33] L. Casnedi, O. Cocco, P. Meloni, G. Pia, Water Absorption Properties of Cement Pastes: Experimental and Modelling Inspections, Advances in Materials Science and Engineering 2018 (2018) 1–9.

[34] J. S. Ceballos-Ruano, T. Kupka, D. W. Nicoll, J. W. Benson, M. A.

882 Ioannidis, C. Hansson, M. M. Pintar, Nuclear magnetic resonance mon-
883 itoring of capillary imbibition and diffusion of water into hardened white
884 cement paste, J. Appl. Phys. 91 (2002) 6588.

885 [35] T. Yamaguchi, K. Negishi, S. Hoshino, T. Tanaka, Modeling of diffusive
886 mass transport in micropores in cement based materials, Cem. Conc.
887 Res. 39 (2009) 1149–1155.